Proceedings of IMECE2002
ASME International Mechanical Engineering Congress & Exposition
November 17-22, 2002, New Orleans, Louisiana

IMECE2002-33859

MANUFACTURING OF ELECTRICALLY CONDUCTIVE MICROSTRUCTURES BY DROPWISE PRINTING AND LASER CURING OF NANOPARTICLE-SUSPENSIONS

Bieri, N.R. **Haferl, S.E.** **Poulikakos, D.**

Laboratory of Thermodynamics in Emerging Technologies
Institute of Energy Technology, Department of Mechanical and Process Engineering
Swiss Federal Institute of Technology
http://www.ltnt.ethz.ch
E-mail: poulikakos@ltnt.iet.mavt.ethz.ch

and

Grigoropoulos, C.P.

Department of Mechanical Engineering, University of California, Berkeley

ABSTRACT

A novel method for the manufacturing of electric microconductors for semiconductor and other devices is presented. The method brings together three technologies: controlled (on demand) printing, laser curing, and the employment of nanoparticles of matter, possessing markedly different properties (here, melting point) than their bulk counterparts. A suspension of gold particles in toluene solvent is employed to print electrically conducting line patterns utilizing a modified on demand ink jet printing process. To this end, microdroplets of 80-100 μm diameters are deposited on a moving substrate such that the droplets form continuous lines. Focused laser irradiation is utilized in order to evaporate the solvent, melt the metal nanoparticles in the suspension, and sinter the suspended particles to form continuous, electrically conducting gold microlines on a substrate. The ultra fine particles in the suspension have a diameter size range of 2 – 5 nm. Due to curvature effects of such small particles, the melting point is markedly lower (400°C) than that of bulk gold (1063°C). Thermodynamic aspects of the effect of particle size on the melting and evaporation temperatures of gold and toluene, respectively, are discussed in the paper.

The structure and line width of the cured line as a function of the laser irradiation power and stage velocity are reported in detail. Preliminary measurements of the electrical conductivity are represented.

Keywords: Nanoparticle-Suspensions, Laser Curing, Micro-printing

INTRODUCTION

The need-driven trend in electronics manufacturing is to constantly develop smaller and tighter packed components. The demand for methods producing ever smaller structures is growing. The present work presents a novel technique producing conducting nano-structured microlines. Drop-on-demand ink jet technology is used to print two dimensional micropatterns out of a suspension containing nanoparticles [1]. The particles are heated up and melted within the carrier-liquid by an argon ion laser focused on the printed line. The volatile liquid solvent evaporates and the nanoparticles are sintered together forming a continuous line.

The advantages compared to current manufacturing methods of printed wiring or circuit boards are many-fold. This method saves expensive materials by only depositing material at desired places on the substrate. Conventional methods apply a metal coating over the entire substrate, followed by a photoresist. A mask of the line pattern is placed on the photoresist. After exposure, the developed photoresist prevents the covered metal from being etched away in a chemical bath. This chemical etching produces highly toxic waste. Moreover, these processes feature an unfavorable efficiency in the use of precious material. Second, the entire procedure is labor-intensive, time-consuming and therefore expensive. To be

profitable large quantities have to be produced. The novel process presented herein is straightforward and fast. The desired pattern can be designed with appropriate CAD/CNC software and suits very well for small production and runs.

Fig. 1 Printed and curded ETH Logo compared with the head of a match. The width of the lines is 62 μm.

THEORETICAL CONCEPTS AND PROCESS PARAMETER SELECTION

The reason why nanoparticle suspensions are employed instead of molten bulk material or bigger particles is the fact that nanoparticles possess different properties than their bulk counterpart. An explanation for this difference in thermo-physical behavior is based on the ratio between surface atoms and inner phase atoms for nanoparticle systems. In a gold particle of 4 nm diameter, 40 percent of the atoms are surface atoms. The ratio of atoms at the surface, N_S, and the total number of atoms, N, of a particle is inversely proportional to radius of the particle:

$$\frac{N_S}{N} \sim \frac{1}{r}$$

The energy of atoms at the surface differs from the energy of inner atoms. The small radius of curvature and finite size of the particle precipitate the influence of the surface atoms. Thermodynamic properties such as the melting and boiling points drastically differ from the bulk properties. The reduction of the melting temperature towards smaller particle sizes is of interest to the present work. This thermodynamic size effect was reported and experimentally investigated by Pawlow, Gladkich, Peppiatt and Buffat [2-5]. Various phenomenological models have been developed [2, 5-6] to describe the reduction of the melting temperature. Kofman et al. [7] proposed a model on the reduction of the melting temperature based on the minimization of the free energy. Accordingly, the complete melting of a solid takes place at a reduced melting temperature T_M:

$$\frac{\Delta T_M}{T_0} = \frac{2\gamma_{SL}}{\rho LR}\left(\gamma_{SV} - \gamma_{LV}\right) \qquad \Delta T_M = T_0 - T_M$$

Surface melting, represented by a stable melt layer at the nanoparticle surface, occurs at a reduced melting temperature T_{SM}:

$$\frac{\Delta T_{SM}}{T_0} = \frac{2\gamma_{SL}}{\rho L(R-r)}\left(1-e^{-\delta/\xi}\right) + \frac{S'R^2}{\rho L\xi(R-r)^2}e^{-\delta/\xi}$$

with $S' = \gamma_{SV} - \left[\gamma_{SL} + \gamma_{LV}\left(\frac{R-\delta}{R}\right)^2\right]$; $\Delta T_{SM} = T_0 - T_{SM}$; $\xi = 6.3$ Å

is an estimate for the short range interaction distances in gold.

The present work employs gold nanoparticles suspended in toluene. The average size of the particles is 2-5 nm and is assumed to be spherical. The transmission electron micrograph in Fig. 1 shows images of the utilized commercially available solution with 30wt% gold. Hence, the advantage of nanoparticles lies both in the reduced melting point and the possibility to create highly loaded suspensions for ink jet piezoelectrically driven printing processes. Liquid gold could not be used with this technique due to its high melting point of 1064°C.

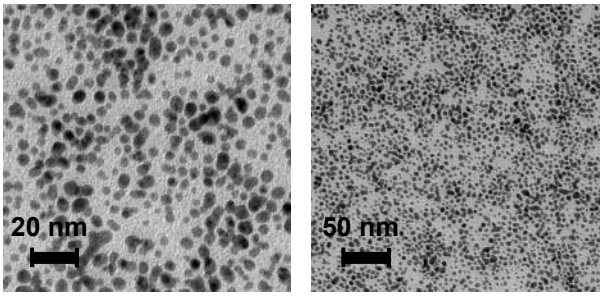

Fig. 2 Picture of the used gold nanoparticle suspension taken by Transmission Electron Microscopy.

As mentioned above, the gold microlines are manufactured by curing the deposited suspension of nanoparticles and carrier liquid. To quantify the laser energy coupling with the nanoparticle suspension, good knowledge of the optical behavior is of central importance. To determine the optical properties of ultra-fine gold particles dispersed in toluene it is necessary to study the scattering behavior of the mixture. The absorption depth is thereby the most important property. It quantifies how deep radiation penetrates into a medium until it is totally absorbed. The absorption depth was calculated with Rayleigh Scattering, Mie Scattering and effective medium theory [8] in order to determine the wavelength at which the radiation is entirely absorbed at 1 μm below the surface of the carrier liquid. This length was selected because it represents a process whereby the radiant energy causing the liquid evaporation and nanoparticle curing is absorbed practically at the surface of the deposited solution. Evaporation from large absorption depths is expected to cause structural problems to the printed lines.

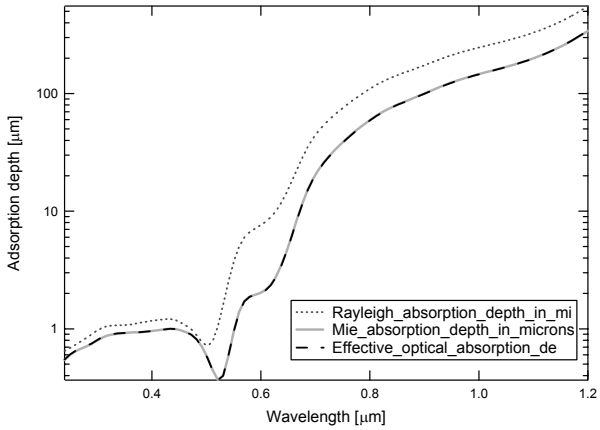

Fig. 3 Absorption depth calculated with different models for NSP of 30wt% gold nanoparticles with average diameter of 5nm suspended in toluene.

It is important to note that only the gold particles are absorbing the laser irradiation; the solvent is translucent. The optical data for gold over the whole spectrum were taken from [9].

The results of the different models matched very well and gave an absorption depth of ~1 μm at wavelengths in the range of 0.35 to about 0.5 μm. Thus, a blue argon laser with $\lambda = 488$ nm was chosen for curing purposes. Because the entire energy of the laser irradiation is absorbed by the gold particles in the first 1 μm of the suspension layer, almost no energy is lost to the solvent and the substrate except through heat conduction. Because of this moderate heat load to the surroundings, even thermally unstable substrates can be employed.

NOMENCLATURE

D	droplet diameter [mm]
f	Printing speed [1/s]
f_l	Focal length [mm]
f_d	Focal diameter [μm]
L	latent heat of fusion [J/kg]
N	number of atoms contained in a particle [-]
N_S	number of atoms at the surface of a particle [-]
P_L	Laser power [mW]
R	particle radius [m]
T_0	melting temperature of the bulk material [K]
T_M	reduced melting temperature of entire melting [K]
T_{SM}	reduced melting temperature of surface melting [K]
U	Stage velocity [mm/s]
V	droplet velocity [m/s]

Greek symbols

δ	thickness of the molten layer [m]
γ_{SV}	surface tension between solid and vapor [J/m^2]
γ_{SL}	surface tension between solid and liquid [J/m^2]
γ_{LV}	surface tension between liquid and vapor [J/m^2]
γ_{SV}	surface tension between solid and vapor [J/m^2]
ρ	density [kg/m^3]
ξ	short range interaction distances [m]

EXPERIMENTS

Droplet Generation and Deposition Setup

To generate and deposit microdroplets of the nanoparticle-suspension (NPS), a piezoelectrically driven micro droplet jetting device was built based on a similar jetting device used for picoliter size solder droplets [10]. This piezoelectric jetting device allows for the generation of monodispersed droplets at demand with diameters in the range of 60-100 μm. The procedure of generating a droplet can be described as follows: By applying an electric pulse to a piezoelectric ceramic tube enclosing a glass capillary containing the NPS, a microdroplet is ejected at demand. The electric pulse shape [11, 12] is thereby of particular importance to control the size, velocity and stability of the generated droplets especially to avoid satellite droplets. The suspension is filled into small reservoir situated above the glass capillary by a syringe and is sealed leak-proof. To prevent the NPS from leaking out of the glass capillary tube due to the strong wettability of the glass capillary by the toluene, (the carrier liquid of the gold nanoparticles), a low vacuum of the order of 10 mbar is sustained in the reservoir. A constant extraction by suction would end in successive evaporation of the toluene and a coagulation of the suspension. Therefore, a magnetic valve with a control system is installed between the reservoir and the vacuum pump. The capacity of the pump is regulated by two hand-controlled needle valves. During standstill periods the NPS tends to clog the orifice. With a short nitrogen gas puff the orifice is cleared again. This cleaning procedure is controlled by a pressure valve to regulate the needed nitrogen backpressure and a magnetic valve to produce a short impulse.

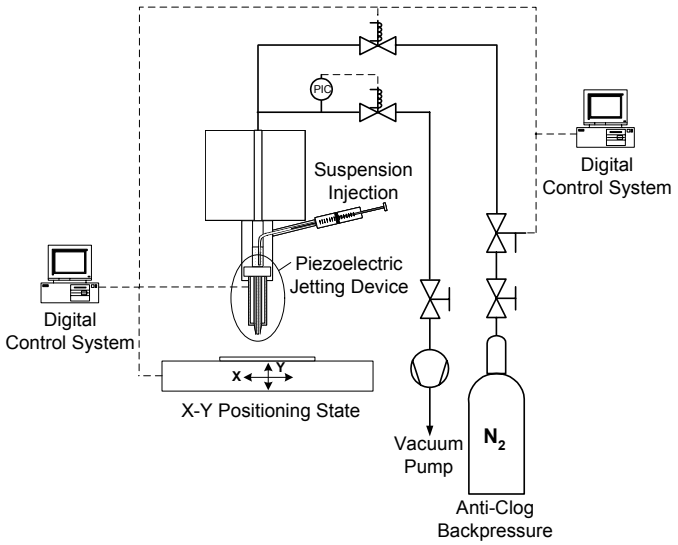

Fig. 4 Schematic of the NPS microdroplet generation and deposition apparatus.

To print lines and various two-dimensional patterns, the substrate is placed on a x-, y-, z-precision positioning stage. The velocity of the stage determines how the droplets are deposited on the substrate, how much they overlap or if they do not even touch each other. The uniform substrates are fixed on a surface mounting placed on the z-translation stage. The jetting device and the positioning stage are controlled by a digital control system. Flash video microscopy is used to record and monitor the droplet generation process, the droplet size, droplet velocity and the prevention of satellite droplets as described in Yarin [13].

Laser Curing Setup

The experimental setup for the curing process consists of an argon ion laser as well as fiber optics to guide the laser beam safely to the experiment setup. The beam is expanded prior to focusing to achieve spot sizes in the range of 10 to 100 μm with a focal waist as long as possible. A beamsplitter is employed to monitor the laser power simultaneously. The printing (including the positioning) and curing processes are synchronized by a digital control system which controls the printing process and a mechanical shutter placed between the argon laser and the fiber optic coupling system. The laser beam is focused at the printed line, preferably close to the point of droplet impact. A typical experiment cycle starts with a cleaning pulse of nitrogen to de-clog the orifice at the free end

of the glass capillary. Upon initiation of the droplet generation sequence, the mechanical laser shutter opens and the positioning stage moves the substrate according to the pre-programmed line pattern.

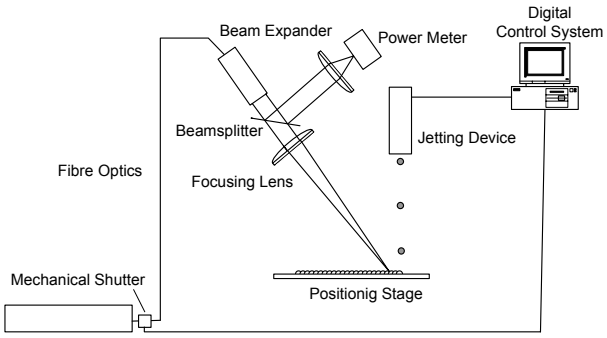

Fig. 5 Schematic of the laser curing setup.

RESULTS AND DISCUSSION

A number of parameters can be identified influencing the properties of the manufactured conductor. Among these are the droplet diameter, droplet velocity, laser power, exposure time to the laser as a function of the stage velocity and the focus diameter of the laser. The herein presented work focuses mostly on the influence of the laser power and the stage velocity on the topology of the cured micro-conductors. Simple measurements of the specific electrical resistance of the cured lines have also been conducted

A. Geometry of Cured Conductors

The laser power is varied between 50-500 mW at two different velocities. The cured lines are analyzed by optical microscopy and atomic force microscopy (AFM). The process parameters are listed in Table I. In Fig. 6 a review is given over the conducted experiments. The width of the line cured at 50 mW and 2 mm/s corresponds to the focal diameter of the laser. At 1 mm/s the heat input at identical laser power increases and is indicated by the greater width of the cured line (Fig. 7a and 7b). The line width is increasing with increasing heat input. The letters correspond to the ones in Fig. 7 where the structure determined by AFM is compared to the structure taken by optical microscopy. With AFM it is possible to record the profiles of the cured lines with nanometer resolution. The two graphs between the AFM and light microscopy images show the AFM profiles of the conductors. The first graph shows height vs. distance across the width of the printed line and the second compares profiles taken at three different locations indicated by the horizontal lines

Table I

Droplet diameter D [mm]	90
Droplet velocity V [m/s]	1.8
Printing speed f [1/s]	15
Focal length f_l [mm]	250
Focal diameter f_d [μm]	15
Stage velocity U [mm/s]	1; 2
Laser power P_L [mW]	50-500

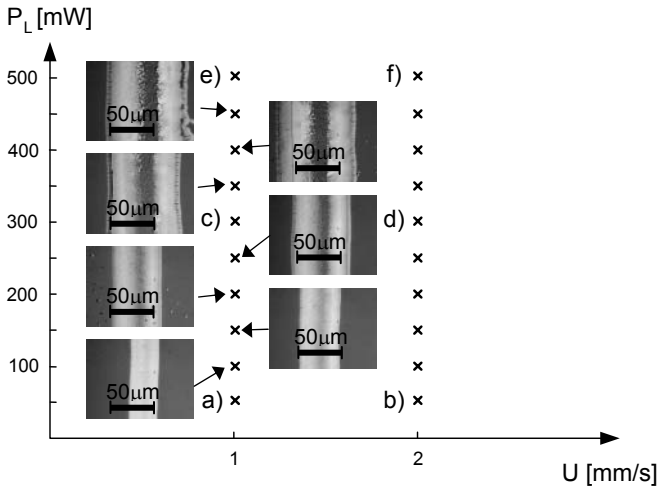

Fig. 6 Review over conducted experiments. Influence of laser power on line width of cured lines. The letters a-f correspond to the pictures in Fig. 7 with the same labels.

In addition to the width, the geometry and the surface topography of the conductor change with increasing laser power. This effect bears some similarity to the described and investigated by Bennett et al. [14] regarding laser texturing of surfaces. From the AFM profiles in Fig. 7a) and 7b), the bowl shape geometry can be observed. The rest of the frames resemble to a sombrero shape. The different shapes are attributed to the Marangoni effect. This effect accounts for the convective motion driven by local changes in surface tension. Surface tension is assumed to be a function of temperature and nanoparticle surface concentration. In Fig. 7a) and 7b) the laser (Gaussian power distribution), which is focused at the center of the line cross section, raises the temperature at the focal point region resulting in a decrease of surface tension. The particles in the solution are dragged towards the colder outer region by thermocapillary forces, creating the rims on both sides of the conductor. At higher laser power, the solvent evaporates faster (and more violently) in the region of the focal point of the laser causing a higher concentration of gold particles in this middle region and an increase of surface tension. This concentration-driven force possibly reverses the topography effects of the thermocapillary forces in the center of the conductor and a hill region is formed. However, thermocapillarity prevails at both sides of the gold line. The constant increase in width with increasing power results from heat conduction because of the higher energy input. During the curing process, a vivid evaporation (the toluene vapor produced was clearly visible) of the solvent at high laser power possibly explains the rough surface topography line in the central region. A detailed investigation describing and quantifying the observed phenomena will be the topic of future work

a) 50 mW, 1 mm/s

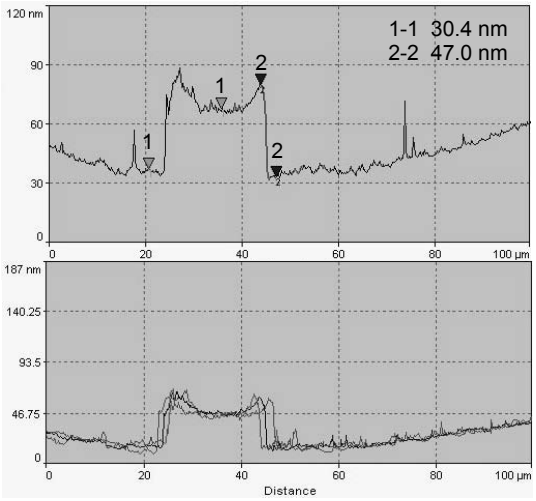

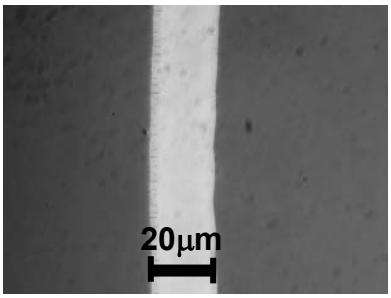

b) 50 mW, 2 mm/s

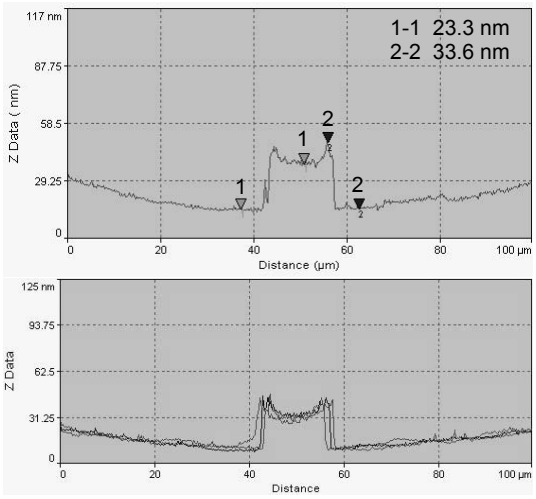

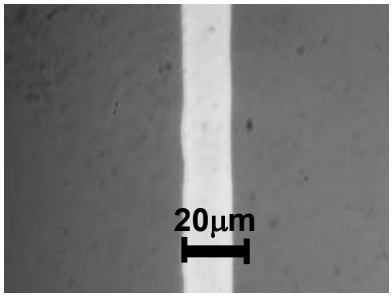

c) 300 mW, 1 mm/s

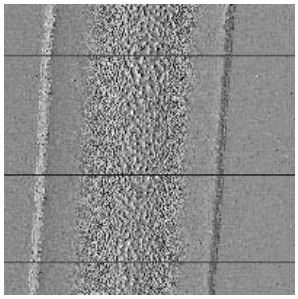

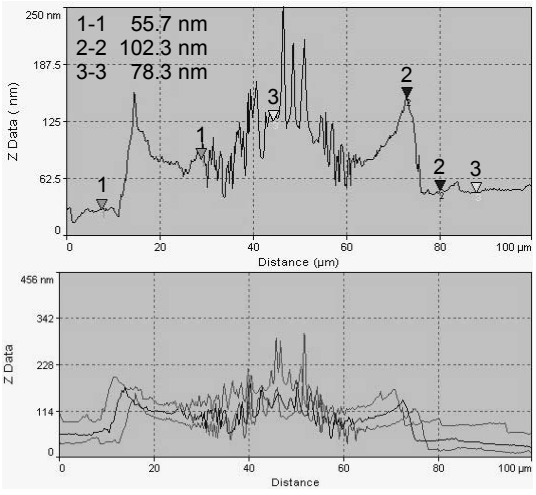

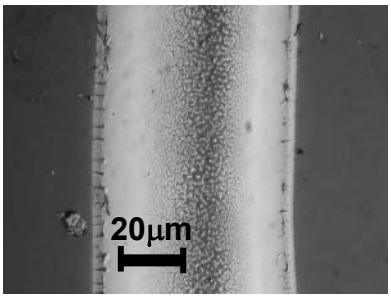

d) 300 mW, 2 mm/s

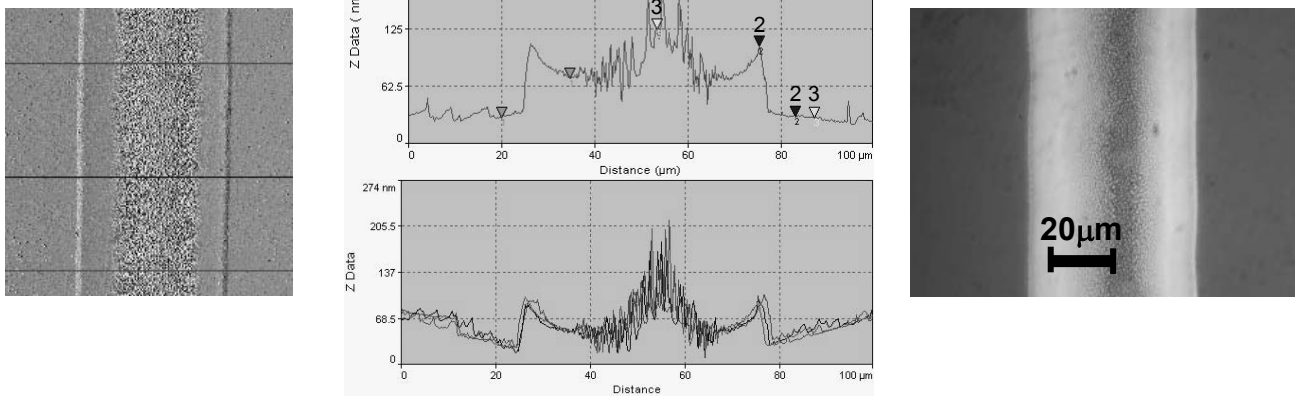

e) 500 mW, 1 mm/s

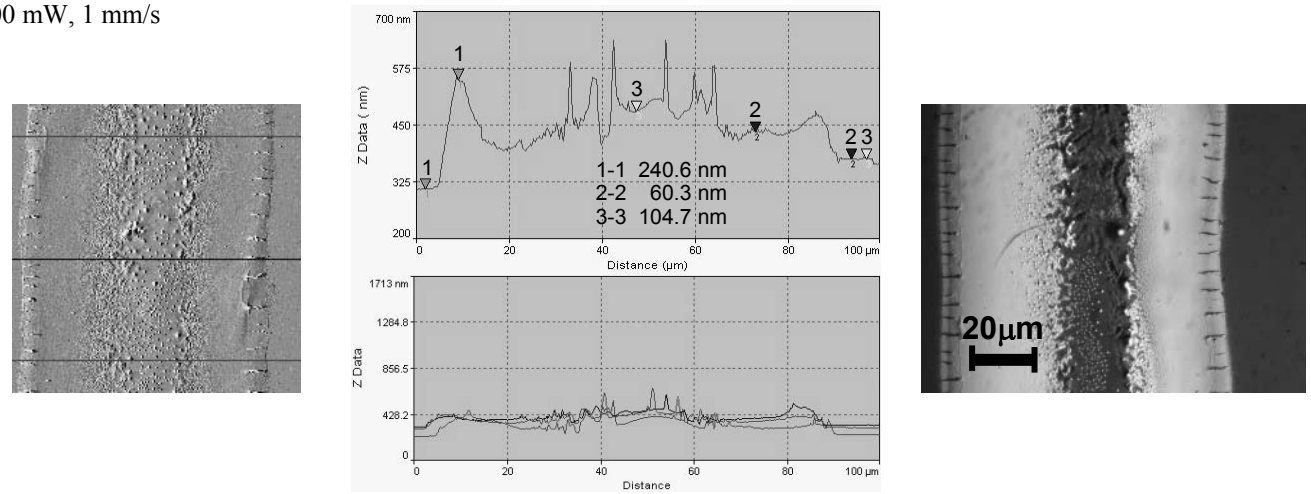

f) 500 mW, 1 mm/s

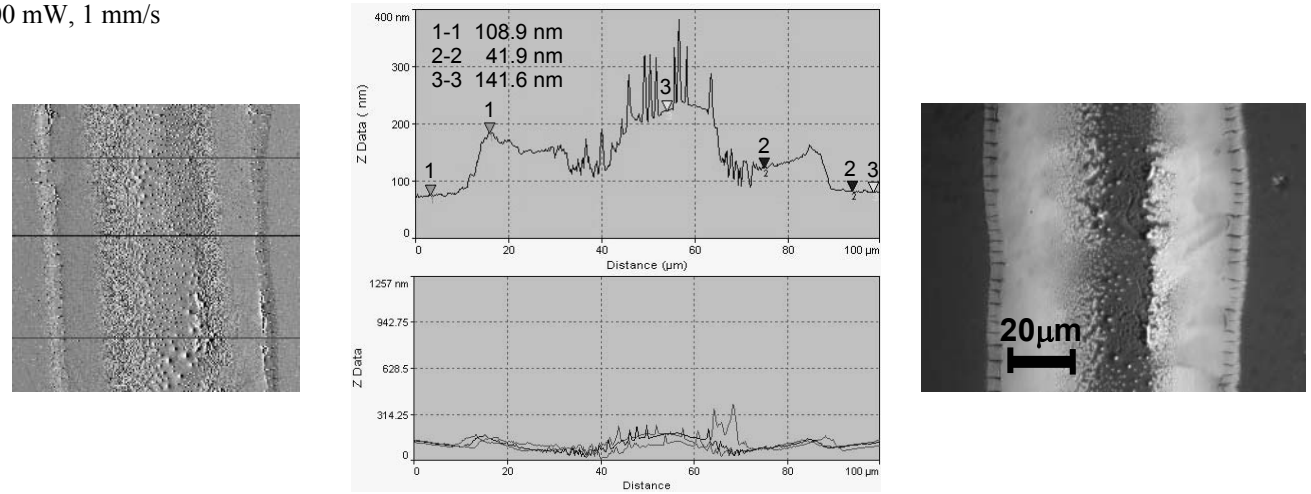

Fig. 7 Optical microscopy and AFM pictures with heights profiles of different laser powers and stage velocities: a) 50 mW; 1 mm/s b) 50 mW; 2 mm/s c) 300 mW; 1 mm/s d) 300 mW; 2 mm/s e) 500 mW; 1 mm/s f) 500 mW; 2 mm

B. Specific Electrical Resistance

One of the objectives of this work is the manufacturing of electrically conducting gold microlines. Therefore, the determination of the specific electrical resistance of the produced structures depending on laser power, exposure time and focus diameter of the laser is of importance. Preliminary measurements conducted with a measuring bridge (Philips MP6303) yielded a specific electrical resistance of 4.3×10^{-5} Ωcm for gold conductors cured with 300 mW and 1 mm/s. For curing with 500mW and 1 mm/s, the specific electrical resistance is 3.8×10^{-5} Ωcm. These values are comparable with the results of cured and sintered silver NPS in an oven [1]. These preliminary measurements are not corrected for contact resistance; thermal influences etc. and should only give a first impression of the possibilities to utilize the cured gold lines as conductor.

ACKNOWLEDGMENTS

This work has been partially supported by the Swiss National Science Foundation (Grant No. 2000-063580.00).

REFERENCES

1. Szczech, J.B., Megaridis, C.M., Gamota, D.R., and Zhang, J., 2002, "Fine-Line Conductor Manufacturing Using Drop-on-Demand PZT Printing Technology," IEEE Transactions on Electronics Packaging Manufacturing, **25**, (1), pp. 1-8.
2. Pawlow, P., 1909, "Über die Abhängigkeit des Schmelzpunktes von der Oberflächenenergie eines festen Körpers," Zeitschrift für physikalische Chemie, **65**, pp. 1-35.
3. Gladkich, N.T., Niederma.R, and Spiegel, K., 1966, "Nachweis Grosser Schmelzpunktserniedrigungen bei Dünnen Metallschichten," Physica Status Solidi, **15**, (1), pp. 181-191.
4. Peppiatt, S.J. and Sambles, J.R., 1975, "Melting of Small Particles .1. Lead," Proceedings of the Royal Society of London Series A - Mathematical Physical and Engineering Sciences, **345**, (1642), pp. 387-390.
5. Buffat Ph. and Borel J.P., 1975, "Size effect on the melting temperature of gold particles," Physical Review A, **13**, (6), pp. 2287-2298.
6. Hanszen, K.J., 1960, "Theoretische Untersuchungen über den Schmelzpunkt kleiner Kügelchen - Ein Beitrag zur Thermodynamik der Grenzflächen," Zeitschrift für Physik, **157**, (5), pp. 523-553.
7. Kofman, R., Cheyssac, P., Aouaj, A., Lereah, Y., Deutscher, G., Bendavid, T., Penisson, J.M., and Bourret, A., 1994, "Surface Melting Enhanced by Curvature Effects," Surface Science, **303**, (1-2), pp. 231-246.
8. Bohren, C.F. and Huffman, D.R., 1983, Absorption and Scattering of Light by Small Particles, John Wiley, New York.
9. Palik, E.D., 1991, Handbook of optical constants of solids II, Academic Press, Inc., San Diego.
10. Attinger, D., Zhao, Z., and Poulikakos, D., 2000, "An Experimental Study of Molten Microdroplet Surface Deposition and Solidification: Transient Behavior and Wetting Angle Dynamics," Journal of Heat Transfer-Transactions of the Asme, **122**, pp. 544-556.
11. Hayes, D.J., Wallace, D.B., and Boldman, M.T.,1992, "Picoliter Solder Droplet Dispensing," Proceedings, ISHM'92, San Francisco, California, pp. 316-321.
12. Hayes, D.J. and Wallace, D.B., 1998, "Solder Jet Printing:Wafer Bumping and CSP Applications," Chip Scale Review, **2**, (4), pp. 75-80.
13. Yarin, A.L. and Weiss, D.A., 1995, "Impact of Drops on Solid-Surfaces - Self-Similar Capillary Waves, and Splashing as a New-Type of Kinematic Discontinuity," Journal of Fluid Mechanics, **283**, pp. 141-173.
14. Bennett, T.D., Krajnovich, D.J., Grigoropoulos, C.P., Baumgart, P., and Tam, A.C., 1997, "Marangoni mechanism in pulsed laser texturing of magnetic disk substrates," Journal of Heat Transfer-Transactions of the ASME, **119**, (3), pp. 589-596.